Macromolecules

pubs.acs.org/Macromolecules Article

Two Sides of the Same Coin: A Unified Theoretical Treatment of Polyelectrolyte Complexation in Solution and Layer-by-Layer Films

Gabriel Debais and Mario Tagliazucchi*

Cite This: *Macromolecules* 2022, 55, 5263−5275 Read Online

ACCESS | Metrics & More | Article Recommendations | Supporting Information

ABSTRACT: Polyelectrolyte coacervates, obtained by mixing solutions of oppositely charged polyions, and layer-by-layer films, produced by sequential adsorption of polyelectrolytes on a surface, are two types of closely related soft materials. While both types of materials are produced by polyelectrolyte complexation, their theoretical description had so far followed divergent paths. This work reports a unifying theoretical treatment of polyelectrolyte complexation in solution and layer-by-layer self-assembled thin films using a molecular theory that describes polyelectrolyte complexation by using a chemical-equilibrium formalism. The theory is shown to predict both the phase diagrams of polyelectrolyte mixtures in solution and the formation of layer-by-layer thin films in good agreement with experimental evidence. In the latter case, the theory correctly captures the effects of solution pH and ionic strength on the mass of the deposited films as well as the possibility of layer-by-layer deposition without full charge reversal at extreme pHs. The theory is then used to revisit the "universal curve" for the effect of salt concentration on layer-by-layer deposition previously proposed on experimental grounds by Salehi et al. [*Macromolecules* **2015**, *48*, 400−409]. This universal curve makes predictions about the growth rate of a layer-by-layer film for a given polyanion/polycation pair by using only information obtained from a mixture of the same polyelectrolytes in solution, thereby linking both phenomena. Our theoretical results confirm the validity of the curve. This achievement demonstrates the practical importance of describing polyelectrolyte coacervates and multilayer films within a unified theoretical framework.

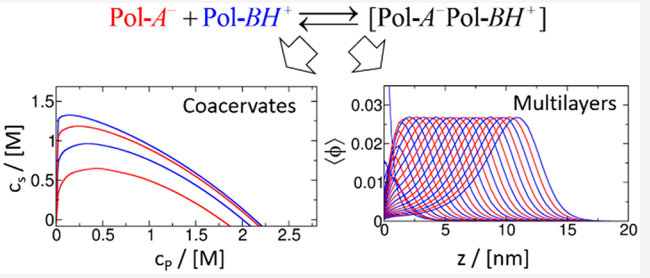

1. INTRODUCTION

The complexation of oppositely charged macromolecules gives rise to two very important classes of soft materials: polyelectrolyte (PE) multilayer thin films[1−4] and PE coacervates.[5−8] The technological relevance of these materials has triggered efforts to model and predict their properties and the effect of processing variables on their microscopic organization. Even though PE complexation is behind the formation of both materials, previous theoretical and simulation work addressed PE multilayers and coacervates independently, which made it difficult to establish connections between the properties of both materials. In this work, we introduce the first unifying theoretical study of PE complexation in solution and in layer-by-layer (LbL) thin films.

Coacervates are obtained by mixing solutions of oppositely charged PEs.[5,7] Stoichiometric mixtures of oppositely charged PEs of similar molecular weight yield electrically neutral complexes that separate from solution, forming a PE-rich phase known as a coacervate.[7] In many conditions, coacervates are viscous liquids instead of solids—a fact that was explained by van der Gutch et al. in terms of the rather small cohesive energy (a few k_BT per chain) between electrically neutral PE complexes.[7] However, this small cohesive energy should not be mistaken with the energy required to break the complexes: the energy to separate the oppositely charged polyions can be as large as hundreds of k_BT per chain at low salt concentrations.[9] This energy quickly decreases when increasing salt concentration, and therefore PE coacervates can be dissolved by increasing the ionic strength of the solution.[7,10−13]

The LbL deposition of PE multilayers leverages the formation of PE complexes to build up thin films by the alternate adsorption of oppositely charged PEs.[1,2] The thickness per layer of LbL films dramatically depends on solution conditions, such as pH[14−16] and ionic strength.[16−22] Some key observations may seem counterintuitive *a priori*. For example, increasing ionic strength, which is known to destabilize PE complexes, as discussed above, initially leads to an increase in film thickness.[16−22]

PE complexation is mainly an entropic phenomenon: the association of a polycation and a polyanion results in the release of the small counterions that neutralize the PE charges

Received: February 2, 2022
Revised: May 2, 2022
Published: June 7, 2022

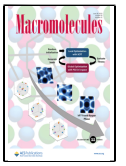

https://doi.org/10.1021/acs.macromol.2c00250
Macromolecules 2022, 55, 5263−5275

before mixing.[5,23−27] This process, known as counterion release, can be summarized with the following reaction:

$$\text{Pol-A}^{-}\text{Na}^{+} + \text{Pol-BH}^{+}\text{Cl}^{-} \rightarrow [\text{Pol-A}^{-}\text{Pol-BH}^{+}] + \text{Na}^{+} + \text{Cl}^{-} \quad (1)$$

where Pol-A^- and Pol-BH^+ denote the polyanion (deprotonated polyacid) and the polycation (protonated polybase), respectively. Note that the entropy gained by the release of salt ions depends on the solution salt concentration: the higher the salt concentration, the lesser the entropy gained in the process described by eq 1. Thus, PE complexation can reversed by a large-enough increase in the ionic strength, which leads to the rupture of polyion−polyion pairs:[9,28,29]

$$[\text{Pol-A}^{-}\text{Pol-BH}^{+}] + \text{Na}^{+} + \text{Cl}^{-} \rightarrow \text{Pol-A}^{-}\text{Na}^{+} + \text{Pol-BH}^{+}\text{Cl}^{-} \quad (2)$$

This mechanism explains the dissolution of coacervates and LbL films at large salt concentrations. Even at small salt concentrations the process in eq 2 leads to the partial rupture of polyion−polyion ion pairs in interpolyelectrolyte complexes, thereby doping the complexes with small salt ions.[28,30]

Molecular dynamics (MD) and Monte Carlo simulations[11,25,27,31−33] correctly capture PE complexation, although these methods are in general too expensive for systematic explorations. For example, there are only a few recent reports of the construction of phase diagrams of PE coacervates using MD.[11,34] On the other hand, the first theoretical treatments of PE coacervation in solution date from the 1950s.[35] To successfully capture PE complexation and its consequences, a theoretical approach must treat electrostatic interactions beyond the mean-field level.[36,37] The earliest description of PE coacervation, the Voorn−Overbeek theory,[35] introduced a term modeling the Debye−Hückel contribution to the free energy which accounted for the attraction between oppositely charged polyions. However, to achieve good agreement with experiments, it is also necessary to include into this theory a Flory−Huggins contribution, which models nonelectrostatic interactions (and introduces fitting parameters into the theory).[7] More recent theories of PE complexation include the random phase approximation,[38−41] field theoretical methods,[42,43] the polymer reference interaction site model (PRISM),[44] the liquid-state theory,[45] and the chemical equilibrium formalism.[12,37,46,47] The latter theory describes PE complexation and counterion binding as chemical equilibria reactions, which results in a very intuitive description, but requires to know the values of the equilibrium constants. We show here that these constants can be successfully obtained by fitting the phase diagrams of PE mixtures in solution.

The formation of LbL films has also been theoretically studied,[41,48−50] although to a lesser degree than coacervates in solution. Interestingly, the understanding of PE coacervation and LbL deposition had advanced in parallel, and very few attempts were done to achieve unified pictures for both phenomena.[16,51] In an interesting step in this direction, Salehi and co-workers proposed an "universal curve" for the effect of ionic strength on LbL deposition.[16]

We developed in this work a molecular theory (MOLT) that is based on the molecular theory previously developed by Szleifer and co-workers[52,53] and our previous work on LbL adsorption[54] and the chemical equilibrium formalism for PE pairing.[37] We then applied this theory to PE coacervates in solution and LbL multilayer thin films. We first fit the phase diagrams of PE mixtures in solution, and then, using the resulting set of fitting parameters, we successfully predicted the LbL growth of PE multilayers. The theory predicts many important experimental trends: (i) the nonmonotonic effects of pH and salt concentration on the mass of deposited LbL films, (ii) the reversal of surface charge upon the addition of a layer in most experimental conditions, and (iii) the possibility of successful deposition even in the absence of full charge reversal at extreme pH values. To demonstrate the importance of describing PE coacervation and LbL deposition within the same theoretical framework, we also revisited and theoretically confirmed the "universal curve" for the effect of salt concentration on LbL growth previously proposed by Salehi, Larson, and co-workers based on experimental grounds.[16]

2. THEORETICAL METHODS

2.1. Formulation of the Molecular Theory for PE Association. We will start the description of our theory by analyzing the thermodynamics of a mixture of polyanions and polycations in the presence of a flat surface. We will then show how that theory can be used to model LbL film assembly and PE mixtures in solution. This approach allows us to model PE complexation in solution and LbL deposition within the same theoretical framework. Figure 1 shows a scheme of the system,

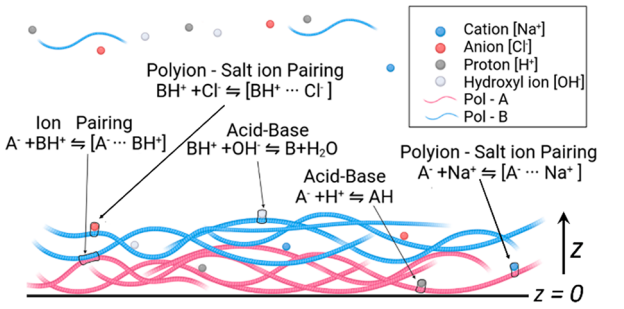

Figure 1. Our theory models a mixture of a polyacid (Pol-A) and a polybase (Pol-B) in solution or on a flat surface. The solution also contains solvent (water) molecules, salt ions (Na^+ and Cl^-), hydroxyl ions (OH^-), and protons (H^+). The monomers in each of these polyelectrolytes can be in four different chemical states, which are related by chemical equilibria reactions. These states are (i) ionized and unassociated (A^- for Pol-A and BH^+ for Pol-B), (ii) neutral (HA and B), (iii) ionized and associated with salt ions (A^-Na^+ and BH^+Cl^-), and (iv) ionized and forming a PE complex ($[A^-\cdots BH^+]$). In the case of layer-by-layer adsorption, the substrate (impenetrable wall for the polyelectrolytes) is located at $z = 0$.

explicitly indicating the species present in the bulk solution: solvent (water), protons (H^+), hydroxyl ions (OH^-), salt anions (Cl^-), and salt cations (Na^+). Pol-A and Pol-B represent the polyanion and polycation, which we model as chains of coarse-grained A-type or B-type beads. Each of these beads maps a single chemical monomer. The flat surface breaks the symmetry of the system, and therefore all structural properties are assumed to depend on z, the direction normal to the surface. Homogeneity will be assumed on each plane parallel to the surface.

Without lack of generality, in this section we will formulate the theory for a system where Pol-A is in solution and there is a Pol-A/Pol-B predeposited film on the surface. Our theoretical description starts off with the Helmholtz free energy functional for the system per unit area:

https://doi.org/10.1021/acs.macromol.2c00250
Macromolecules 2022, 55, 5263−5275

$$\frac{\beta F}{A} = -\frac{S_{\text{Trans}}}{Ak_B} + \frac{\beta F_{\text{Int}}}{A} + \frac{\beta F_{\text{Chem}}}{A} - \frac{S_{\text{Conf}}}{Ak_B} + \frac{\beta F_{\text{vdW}}}{A} + \frac{\beta F_{\text{Elect}}}{A} \tag{3}$$

where A is the area of the system, k_B is Boltzmann's constant, and $\beta = 1/k_BT$.

The translational entropy, $-S_{\text{Trans}}/(Ak_B)$, accounts for the contribution of the translational (mixing) free energy for all species in solution

$$-\frac{S_{\text{Trans}}}{Ak_B} = \sum_{\substack{i=H^+,OH^-,s \\ Na^+,Cl^-}} \int \rho_i(z)[\ln(\rho_i(z)v_s) - 1]\, dz + \int \rho_A(z)[\ln(\rho_A(z)v_s) - 1]\, dz \tag{4}$$

where the first term includes the small ions and the solvent and the second one the Pol-A chains in solution, v_s is the solvent volume, and $\rho_i(z)$ is the number density of each species at position z (i.e., $\rho_i(z)$ is the number density of chains of type i). It should be noted that eq 4 contains the translational contribution of Pol-A chains. As we mentioned above, we are formulating the theory assuming that Pol-A is the PE being adsorbed, and thus it is the only polyelectrolyte present in the solution (previously adsorbed Pol-A and Pol-B chains do not contribute to the translational entropy). In those steps involving the adsorption of Pol-B, eq 4 will contain the translational contribution of Pol-B chains instead of Pol-A chains.

The internal free energy (βF_{Int}) contribution contains the standard chemical potential for the different chemical species, and it is given by

$$\frac{\beta F_{\text{int}}}{A} = \sum_{\substack{i=H^+,OH^- \\ Na^+,Cl^-}} \int \rho_i(z)\beta\mu_i^\circ\, dz \tag{5}$$

where μ_i° is the standard chemical potential of species i. Note that the chemical potentials of Pol-A and Pol-B are not included in eq 5 because we include them (at the monomer level) in F_{Chem}, as described next.

The third term in the free energy of the system corresponds to the contribution of the chemical reactions considered by our theory, namely:

(i) Acid–base reactions that model the association of polyanions with protons in solution

$$\text{Pol-AH} \rightleftarrows \text{Pol-A}^- + \text{H}^+ \tag{6}$$

and of polycations with hydroxyl ions

$$\text{Pol-B} + \text{H}_2\text{O} \rightleftarrows \text{Pol-BH}^+ + \text{OH}^- \tag{7}$$

(ii) Formation of interpolyelectrolyte complexes via polyion–polyion ion pairing that models the association between charged acid and basic groups in the PEs:

$$\text{Pol-A}^- + \text{Pol-BH}^+ \rightleftarrows [\text{Pol-A}^-\text{Pol-BH}^+] \tag{8}$$

(iii) Formation of ion–polyion ion pairs between PEs and salt ions that models the association between charged groups in the polyanions and salt cations in solution (i.e., counterion binding)

$$\text{Pol-A}^- + \text{Na}^+ \rightleftarrows [\text{Pol-A}^-\text{Na}^+] \tag{9}$$

and between the polycations and salt anions

$$\text{Pol-BH}^+ + \text{Cl}^- \rightleftarrows [\text{Pol-BH}^+\text{Cl}^-] \tag{10}$$

The free energy contribution that results from these chemical equilibria is[37]

$$\frac{\beta F_{\text{chem}}}{A} = \int \langle n_A(z)\rangle \sum_{j=c,uc,as,as\text{-ion}} f_j^A(z)(\ln(f_j^A(z)) + \beta\mu_j^{\circ,A})\, dz + \int \langle n_B(z)\rangle \sum_{j=c,uc,as,as\text{-ion}} f_j^B(z)(\ln(f_j^B(z)) + \beta\mu_j^{\circ,B})dz - \int \langle n_A(z)\rangle f_{as}^A(z)(\ln(\langle n_A(z)\rangle f_{as}^A(z)v_{AB}) - 1)\, dz \tag{11}$$

where f_j^A and f_j^B are the fractions of monomers of type A and B, respectively, in state j. Following eqs 6–10, the possible states of the monomers are charged (j = c, corresponds to A^- and BH^+), uncharged (j = uc, species AH and B), polyion–polyion ion pairs (j = as, corresponds to the [Pol-A^-···Pol-BH^+] complex), and ion–polyion ion pair (j = as-ion, ANa, and BHCl). $\mu_j^{o,A}$ and $\mu_j^{o,B}$ are the standard chemical potentials for a monomer in each of these states, and the volume v_{AB} is the volume of the complex formed by the association of a negative and a positive monomer, [Pol-A^- ···Pol-BH^+]. The detailed derivation of eq 11 can be found in the Supporting Information of our previous works.[37,54] It should be noted that f_j^A and f_j^B fulfill the condition

$$\sum_{j=c,uc,as,as\text{-ion}} f_j^i(z) = 1 \quad \text{for } i = A, B \tag{12}$$

In eq 11, $\langle n_i(z)\rangle$ is the total concentration of the monomers of each polymer (i = A, B). This concentration can be split into the contribution of the adsorbed layers and that of the polymer in solution being absorbed. For Pol-A (PE being adsorbed)

$$\langle n_A(z)\rangle = \sum_l \langle n_A^{\text{fix},l}(z)\rangle + \int \rho_A(z') \times \sum_\alpha P_A(\alpha, z')n_A(z, z', \alpha)\, dz' \tag{13}$$

and for Pol-B (PE absent in solution)

$$\langle n_B(z)\rangle = \sum_l \langle n_B^{\text{fix},l}(z)\rangle \tag{14}$$

where $\langle n_i^{\text{fix},l}(z)\rangle$ (for i = A, B) is the density profile of the previously adsorbed layer l (the sum over l, therefore, runs over all previously adsorbed layers). In our theory, the density profiles of Pol-A and Pol-B in the preadsorbed layers are assumed to be frozen during the adsorption of the next layer from solution (see below). In other words, $\langle n_i^{\text{fix},l}(z)\rangle$ is fixed, and the free-energy functional will not be minimized with respect to it. The second term on the RHS of eq 13 corresponds to the concentration of Pol-A in solution. In this term, $P_A(\alpha,z')$ is the probability of having the first segment of Pol-A chain at z' in conformation α, and the sum over α runs in principle over all the possible conformations of Pol-A chains (although in practice, we use a large representative set of randomly generated conformations). In that term, $n_A(z,z',\alpha)$ dz is defined as the number of segments that a Pol-A chain with its first segment at z' has between z and $z + dz$.

The fourth term, $-S_{\text{Conf}}/(Ak_B)$, is the contribution of the conformational entropy of the adsorbed chain, and it is given by the equation

https://doi.org/10.1021/acs.macromol.2c00250
Macromolecules 2022, 55, 5263–5275

$$-\frac{S_{\text{Conf}}}{Ak_{\text{B}}} = \int \rho_{\text{A}}(z) \sum_{\alpha} P_{\text{A}}(\alpha, z) \ln(P_{\text{A}}(\alpha, z))\, \text{d}z \tag{15}$$

The term βF_{vdW} represents the effective van der Waals attractions between all polymer beads.[55,56] We model these interactions using the attractive branch of a Lennard-Jones potential:

$$u_{\text{vdW}}(r) = \begin{cases} -4\left(\frac{a}{r}\right)^6 & \text{if } a < r < r_{\text{cutoff}} \\ 0 & \text{otherwise} \end{cases} \tag{16}$$

where a is the bead diameter (segment length, we used a = 0.35 nm) and r_{cutoff} is a cutoff distance (we used r_{cutoff} = 1.25 nm). The vdW attractions result in the following mean-field contribution to the total free energy of the system

$$\frac{\beta F_{\text{vdW}}}{A} = \iint \frac{1}{2}\beta\epsilon g(|z - z'|)(\langle n_{\text{A}}(z)\rangle + \langle n_{\text{B}}(z)\rangle)(\langle n_{\text{A}}(z')\rangle + \langle n_{\text{B}}(z')\rangle)\, \text{d}z\, \text{d}z' \tag{17}$$

where ϵ determines the strength of the interaction and $g(|z - z'|)$ is a parameter that accounts for its geometric dependence[56]

$$g(|z - z'|) = \int_{-\infty}^{\infty}\int_{-\infty}^{\infty} u_{\text{vdW}}([(z - z')^2 + x^2 + y^2]^{1/2})\, \text{d}x\, \text{d}y \tag{18}$$

The last term (βF_{Electro}) is the electrostatic contribution to the free energy

$$\frac{\beta F_{\text{Electro}}}{A} = \beta \int \left(\langle \rho_q(z)\rangle \psi(z) - \frac{1}{2}\varepsilon(\nabla\psi(z))^2\right) \text{d}z \tag{19}$$

where $\psi(z)$ is the electrostatic potential at z and ε is the dielectric permittivity. We assume that ε is independent of z and equal to the dielectric permittivity of bulk water. Previous studies of polyelectrolyte brushes have shown that this approximation has practically no effect on the structure of the system.[52,57] In eq 19, $\langle \rho_q(z)\rangle$ is the total charge density, given by

$$\langle \rho_q(z)\rangle = f_{\text{c}}^{\text{A}}(z) q_{\text{A}} \langle n_{\text{A}}(z)\rangle + f_{\text{c}}^{\text{B}}(z) q_{\text{B}} \langle n_{\text{B}}(z)\rangle + \sum_{i=\text{H}^+,\text{OH}^-,\text{Na}^+,\text{Cl}^-} q_i \rho_i(z) \tag{20}$$

where q_i is the charge of the species i.

At this point, we should mention that the proper thermodynamic potential to model the system is not the Helmholtz free energy F, which considers a fixed number of each chemical species. Instead, a grand-canonical potential should be used, which fixes the chemical potentials of all species in solution. This potential is

$$\beta\omega = \frac{\beta F}{A} - \beta\mu_{\text{A}} \int \rho_{\text{A}}(z)\, \text{d}z - \sum_{\substack{i=\text{H}^+,\text{OH}^-,\text{s} \\ \text{Na}^+,\text{Cl}^-}} \beta\mu_i \int \rho_i(z)\, \text{d}z - \beta\mu_{\text{H}^+} \int f_{\text{uc}}^{\text{A}}(z)\langle n_{\text{A}}(z)\rangle\, \text{d}z - \beta\mu_{\text{OH}^-} \int f_{\text{uc}}^{\text{B}}(z)\langle n_{\text{B}}(z)\rangle\, \text{d}z - \beta\mu_{\text{Na}^+} \int f_{\text{as-ion}}^{\text{A}}(z)\langle n_{\text{A}}(z)\rangle \text{d}z - \beta\mu_{\text{Cl}^-} \int f_{\text{as-ion}}^{\text{B}}(z)\langle n_{\text{B}}(z)\rangle\, \text{d}z \tag{21}$$

In this expression, the second and third terms are related to the chemical potentials of the free species in solution, the fourth and sixth terms account for the protons and salt cations associated with polyacid chains, and the fifth and seventh terms account for the hydroxyl and salt anions associated with the polybase.

The functional extremum of eq 21 needs to be subjected to four constraints. The first of the constraints is the packing restriction, which models steric repulsions as excluded-volume interactions. This constraint is given by

$$\langle n_{\text{A}}(z)\rangle v_{\text{p}} + \langle n_{\text{B}}(z)\rangle v_{\text{p}} + \sum_{\substack{i=\text{H}^+,\text{OH}^-,\text{s} \\ \text{Na}^+,\text{Cl}^-}} \rho_i(z) v_i = 1 \tag{22}$$

The second constraint enforces the stoichiometry of polyion−polyion ion pairs. At each position z, the number of acidic and basic segments involved in polyion−polyion association should be the same:

$$\langle n_{\text{A}}(z)\rangle f_{\text{as}}^{\text{A}}(z) = \langle n_{\text{B}}(z)\rangle f_{\text{as}}^{\text{B}}(z) \tag{23}$$

The third constraint is the normalization of the probability distribution functions for the Pol-A chains in solution, $P_{\text{A}}(\alpha,z)$:

$$\sum_{\alpha} P_{\text{A}}(\alpha, z) = 1 \quad \text{for all } z \tag{24}$$

Finally, the fourth constrain is the global electroneutrality constraint, namely

$$\int \rho_{\text{Q}}(z)\, \text{d}z = 0 \tag{25}$$

The constraints described above are enforced with Lagrange multipliers:

$$\mathcal{L} = \beta\omega + \beta \int \pi(z)(\langle n_{\text{A}}(z)\rangle v_{\text{p}} + \langle n_{\text{B}}(z)\rangle v_{\text{p}} + \sum_{i=\text{H}^+,\text{OH}^-,\text{s},\text{Na}^+\text{Cl}^-} \rho_i(z) v_i - 1)\, \text{d}z + \beta \int \lambda(z)(\langle n_{\text{A}}(z)\rangle f_{\text{as}}^{\text{A}}(z) - \langle n_{\text{B}}(z)\rangle f_{\text{as}}^{\text{B}}(z))\, \text{d}z + \int \beta\xi(z)\rho_{\text{A}}(z) (\sum_{\alpha} P_{\text{A}}(\alpha, z) - 1)\, \text{d}z + \beta\phi \int \rho_{\text{Q}}(z)\, \text{d}z \tag{26}$$

In this expression, the Langrage multiplier $\pi(z)$, which enforces the packing constraint, has the role of a local osmotic pressure and the multiplier $\beta\xi(z)\rho_{\text{A}}(z)$, which enforces the normalization of $P_{\text{A}}(\alpha,z)$, is related to the single-chain partition function of Pol-A (see below). Finally, ϕ is an additive constant to the electrostatic potential, $\psi(z)$, which will be therefore absorbed inside it in this section.[52] Note, however, that in the treatment of PE mixtures in solution, when analyzing the coexistence of two thermodynamic phases (section 2.4), each phase has a different value of ϕ, and their difference gives rise to the Donnan potential between the phases. In those conditions, it is important to explicitly write ϕ in the equations (see section 2.4).

To model the adsorption of Pol-A on a preformed Pol-A/Pol-B film, we find the functional extremum of the functional given by eq 26 with respect to the unknown functions in the theory, namely, $\rho_i(z)$, $P_{\text{A}}(\alpha,z)$, f_j^{A}, $f_j^{\text{B}}(z)$, and $\psi(z)$.

The extremum with respect to the probability $P_{\text{A}}(\alpha,z)$ results in the expression

https://doi.org/10.1021/acs.macromol.2c00250
Macromolecules 2022, 55, 5263−5275

$$P_A(a, z) = \frac{1}{Q_A(z)} \exp\{-\int n_A(z', z, \alpha)[\ln(f_c^A(z')) + \beta\pi(z')v_p + \beta\psi(z')q_A - \int \epsilon g(|z' - z''|)(\langle n_A(z'')\rangle + \langle n_B(z'')\rangle)\, dz'']\, dz'\} \quad (27)$$

where $Q_A(z)$ is the single-chain partition function for Pol-A chains with a first segment at position z, which is related to the Lagrange multiplier $\xi(z)$ by $Q_A(z) = \exp(1 + \beta\xi(z))$.

The extremum with respect to the number density of solvent molecules results in

$$\rho_s(z)v_s = \exp(-\beta\pi(z)v_s) \quad (28)$$

Extremization of eq 26 with respect to the number density of the ions (i = H^+, OH^-, Na^+, Cl^-) yields

$$\rho_i(z)v_s = \exp(-\beta\pi(z)v_i - \beta\psi(z)q_i - \beta\mu_i^\circ + \beta\mu_i) \quad (29)$$

The extremum of $\mathcal{L}$ with respect to the number density of Pol-A results in

$$\rho_A(z)v_s = Q_A(z)\exp(\beta\mu_A) \quad \text{for } i = \text{A, B} \quad (30)$$

We also find the extrema of $\mathcal{L}$ with respect to the fractions of A and B monomers in the different chemical states, $f_j^A(z)$ and $f_j^B(z)$ (j = c, uc, as, as-ion). This procedure results in the acid–base chemical equilibria and the ion–polyion and polyion–polyion association reactions. For the acid groups

$${}^AK_a^\circ = \frac{f_c^A(z)\rho_{H^+}(z)}{f_{uc}^A(z)\rho_s(z)} \quad (31)$$

where ${}^AK_a^o = \exp(-\beta\Delta G^\circ) = \exp(-\beta(\mu_{H^+}^o + \mu_c^{o,A} - \mu_{uc}^{o,A}))$ is the thermodynamic equilibrium constant of the acid–base reaction given by eq 6. In analogy, for the base groups (reaction given by eq 7)

$${}^BK_b^\circ = \frac{f_c^B(z)\rho_{OH^-}(z)}{f_{uc}^B(z)\rho_s(z)} \quad (32)$$

where ${}^BK_b^o = \exp(-\beta\Delta G^\circ) = \exp(-\beta(\mu_{OH^-}^o + \mu_c^{o,B} + \mu_{uc}^{o,B}))$. The thermodynamic constants ${}^AK_a^o$ and ${}^BK_b^o$ can be related to the commonly employed equilibrium constants by using molar reference states for the concentrations by dividing them by a factor $c_0N_Av_s$ /(10^{24} nm^3/dm^3).

The ion–polyion ion-pair association of Pol-A with cations (Na^+), reaction in eq 9, is given by

$${}^AK_{as\text{-}ion}^\circ = \frac{f_{as\text{-}ion}^A(z)(\rho_s(z)v_s)^{v_{Na^+}/v_s}}{f_c^A(z)\rho_{Na^+}(z)v_s} \quad (33)$$

with ${}^AK_{as\text{-}ion}^o = \exp(\beta(\mu_{Na^+}^o - \mu_{as\text{-}ion}^{o,A} + \mu_c^{o,A}))$. For the association of the Pol-B with Cl^- anions (eq 10)

$${}^BK_{as\text{-}ion}^\circ = \frac{f_{as\text{-}ion}^B(z)(\rho_s(z)v_s)^{v_{Cl^-}/v_s}}{f_c^B(z)\rho_{Cl^-}(z)v_s} \quad (34)$$

where ${}^BK_{as\text{-}ion}^o = \exp(\beta(\mu_{Cl^-}^o - \mu_{as\text{-}ion}^{o,B} + \mu_c^{o,B}))$. The thermodynamic constants ${}^AK_{as\text{-}ion}^o$ and ${}^BK_{as\text{-}ion}^o$ can be transformed to association constants by using molar concentrations as reference state by multiplication by $c_0N_Av_{Na^+}$ /(10^{24} nm^3/dm^3).

The polyion–polyion pairing (see eq 8) is given by

$$K_{as}^\circ v_{AB} = \frac{f_{as}^A(z)}{f_c^A(z)f_c^B(z)\langle n_B(z)\rangle} = \frac{f_{as}^B(z)}{f_c^A(z)f_c^B(z)\langle n_A(z)\rangle} \quad (35)$$

where $K_{as}^o = \exp(-\beta(\mu_{as}^{o,A} + \mu_{as}^{o,B} - \mu_c^{o,A} - \mu_c^{o,B}))$. In this case, it is possible to obtain the association constant in the molar reference state, K_{as}, as $K_{as} = K_{as}^o v_{AB}c_0N_A/(10^{24}\ nm^3/dm^3)$.

Finally, the functional extremum with respect to the electrostatic potential, $\psi(z)$, results in

$$\nabla(\varepsilon\nabla\psi(z)) = -\langle\rho_q(z)\rangle \quad (36)$$

Equation 36 is a mean-field analogue of Poisson's equation for electrostatics, where the electrostatic potential and the number density of charges are replaced by their ensemble averages. The boundary conditions for this equation are $\psi(z\to\infty) = 0$ (bulk) and an uncharged surface at $z = 0$:

$$\left.\frac{\partial\psi(z)}{\partial z}\right|_{z=0} = 0 \quad (37)$$

Note that an uncharged surface is used at $z = 0$ because the intrinsic charges of the bare substrate are introduced as a monolayer of B-type segments distributed over the first 0.5 nm from the surface, see next section.

2.2. Discretization and Numerical Solution. To solve the MOLT for LbL self-assembly, eqs 27–35 are inserted into the packing constraint (eq 22), the mean-field Poisson equation (eq 36), and the stoichiometry constraint (eq 23). The resulting equations are discretized in the z direction by using a discretization step of 0.5 nm and solved by using numerical methods. Further information about the discretization and numerical resolution can be found in our previous works.[37,54]

2.3. Procedure for LbL Self-Assembly. We describe now the protocol to model LbL self-assembly with the MOLT described above. We started the construction of the film with a substrate modified with a monolayer of B-type beads. These beads are distributed in the region between $0 < z < 0.5$ nm and have a number density of 0.5 beads/nm^3 (these beads contribute to the sum in eq 14). Note that after a few adsorbed layers the growth of the LbL structure reaches a steady state[54] and becomes independent of the intrinsic charge of the substrate. We modeled the adsorption of Pol-A on the substrate coated by B beads by solving the MOLT and obtaining the equilibrium density profile of Pol-A in the system. We then performed a "rinsing" step, where we kept in the system only the Pol-A chains that have more than N^b_{max} polyion–polyion bonds with previously adsorbed B monomers. Namely, for each conformation (α) and position of the first segment (z') of the Pol-A chain, we first determined the number of polyion–polyion bonds, $N^b(\alpha,z')$, as

$$N^b(\alpha, z') = \int f_{as}^A(z)n_A(z, z', \alpha)\, dz \quad (38)$$

We then determined the density profile of the newly adsorbed layer as

$$\langle n_A^{fix,1}(z)\rangle = \int \rho_A(z') \sum_{\alpha, N^b(\alpha,z')>N^b_{max}} P_A(\alpha, z')n_A(z, z', \alpha)\, dz' \quad (39)$$

Note that in the summation over α we only include conformations that have more than N^b_{max} polyion–polyion bonds. In this work, we used a value of $N^b_{max} = 0.1N$ (where N

https://doi.org/10.1021/acs.macromol.2c00250
Macromolecules 2022, 55, 5263–5275

is the chain length), which was chosen to produce results compatible with experiments. Smaller values of N^{b}_{max} (e.g., N^{b}_{max} = 1 for N = 75) produced density profiles with a long density tail due to dangling, weakly adsorbed chains (see Figure S1 in the Supporting Information). On the other hand, for larger values (e.g., N^{b}_{max} = 20 for N = 75), almost all chains were removed during the rinsing steps, and the LbL process was halted (Figure S1). After the rising step, the process described above was repeated for the adsorption of subsequent layers, alternating Pol-A and Pol-B in the bulk solution.

Note that the rising step is a nonequilibrium process: the rising solution is free of PEs; therefore, thermodynamic equilibrium can only be achieved by fully dissolving the film. To prevent the desorption of preadsorbed layers, we froze their density profiles. In other words, the profile of the first layer (determined from eq 39) was not modified during the adsorption of the second and following layers, and a similar protocol was applied to subsequent layers. Arguably, the lack of relaxation of previously adsorbed chains is a weakness of our theory, but we adopted it because, as we show below, this approximation produces predictions that agree very well with experimental observations and it is very intuitive and simple to use.

2.4. Molecular Theory for a PE Mixture in Solution. We will now show how the theory derived above can be employed to describe the formation of PE coacervates in solution. Because in a bulk solution there is not a privileged direction, all functions become independent of z. Hence, all dependence with z is dropped from previous equations. For example, the translational entropy of the system (eq 4) per unit volume becomes

$$-\frac{S_{Trans}}{Vk_B} = \sum_{\substack{i=H^+,OH^-,s\\ Na^+,Cl^-}} \rho_i[\ln(\rho_i v_s) - 1] + \rho_A[\ln(\rho_A v_s) - 1] + \rho_B[\ln(\rho_B v_s) - 1] \quad (40)$$

Note that this term now contains the translational entropy contributions from both Pol-A (second term on the RHS) and Pol-B (third term) because we now consider a bulk solution containing both PEs. (Here it is important to remember that ρ_A and ρ_B are the number densities of Pol-A and Pol-B chains, not of the respective segments.) The terms βF_{Int} and βF_{Chem}, accounting for the internal free energies and the free-energy contribution from chemical equilibria, are straightforwardly modified for bulk solution by dropping the dependence on z. On the other hand, in bulk solution, $n(\alpha,z,z')$ becomes equal to N (the chain length), and therefore $P(\alpha)$ is constant (within our theory, all chain conformations become equiprobable). Hence, the contribution from the conformational entropy of PE chains in solution (S_{Conf}) becomes constant, and it can be omitted from the free energy functional. Having constant $P(\alpha)$ is expected to be a very good approximation for the coacervate phase because it has been shown that chains in symmetric coacervates have nearly Gaussian conformations.[58,59] It will also be a relatively good approximation in the dilute phase for weak electrostatic interactions (weakly charged chains and/or high salt concentration), although it may introduce an error in the predicted phase diagram for the dilute phase and at very low salt concentrations (where rodlike chain conformations are expected). Therefore, our description of the conformational entropy is expected to be good for high salt concentrations (where polymers have nearly Gaussian statistics in both the coacervate and dilute phases) and to introduce an error in the low salt regime (where the polymers in the dilute phase have rodlike conformations). In the latter case, the conformational entropy should favor the formation of the coacervate; that is, the chains would gain conformational entropy when being transferred from the dilute phase (rodlike conformations) to the coacervate phase (Gaussian conformations). However, we observe that our fit of the experimental data already overestimates the stability of the phase-separated region of the diagram in the dilute branch (see Figure 2). Thus, we

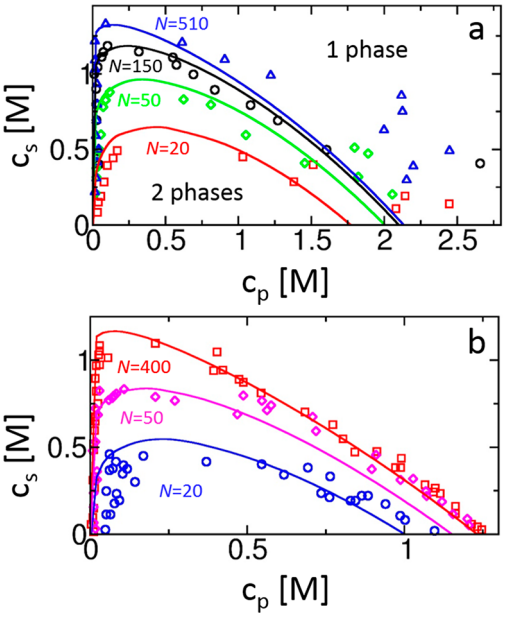

Figure 2. Phase diagrams for PAA/PDMAEMA (a) and poly(lysine)/poly(glutamic acid) (b) as a function of the total molar concentration of polymer (c_p, expressed in terms of the monomer) and salt (c_s). Experimental points correspond to measurements of Spruijt et al.[10] (a) and Li et al.[11] (b, note that this work reported volume fractions, which were transformed to molar concentrations by using the densities reported in the paper) for different chain lengths, N (both PEs have the same length). Solid lines show the predictions of our model for the fitting parameters: (a) K_{as} = 3.55 [M^{-1}], $K_{as\text{-}ion}$ = 1.20 [M^{-1}], ϵ = 0.58 k_BT, v_p = 0.15 nm^3; (b) K_{as} = 5.62 [M^{-1}], $K_{as\text{-}ion}$ = 1.20 [M^{-1}], ϵ = 1.02 k_BT v_p = 0.2 nm^3. Calculation condition: pH = 7.

conclude that the error in the conformational entropy is small compared to the other terms in the free energy. The bulk solution is electroneutral ($\langle\rho_q\rangle$ = 0), and it has a constant (average) electrostatic potential; therefore, the electrostatic contribution (βF_{Elect}) is zero. This approximation reveals the mean-field nature of the term βF_{Elect}, and it stresses the need for explicitly accounting for short-range ion−ion attractions by using the chemical equilibrium formalism.

Following the derivation of the theory for LbL self-assembly, we also consider in this case a Legendre transform of F, the grand-canonical potential ω (eq 21), and, then, introduce the packing (eq 22), stoichiometry (eq 23), and global electroneutrality (eq 24) constraints through the use of Lagrange multipliers. The resulting functional is finally minimized with respect to the scalar variables ρ_i, f^{A}_{j}, and f^{B}_{j}. The minimization with respect to ρ_i leads to equations similar to eqs 28, 29, and 30. In this case, we rearranged the equations to isolate the chemical potential, as it is useful to construct the phase

https://doi.org/10.1021/acs.macromol.2c00250
Macromolecules 2022, 55, 5263−5275

diagram of the system, see below. Therefore, the resulting expressions are

$$\beta\mu_i = \ln(\rho_i v_s) - \frac{N v_p}{v_s}\ln(\rho_s v_s) + N q_i \beta\phi + N \ln(f_c^i) - \beta\epsilon g_{tot} N^2(\rho_A + \rho_B) \quad (41)$$

for i = A, B (the PEs), where

$$g_{tot} = \int g(|z - z'|)\, d(|z - z'|) \quad (42)$$

and

$$\beta\mu_i = \ln(\rho_i v_s) - \frac{v_i}{v_s}\ln(\rho_s v_s) + \beta\mu_i^\circ + \beta\phi q_i \quad \text{for } i = H^+, OH^-, Na^+, Cl^- \quad (43)$$

for the ions.

We also obtain the same chemical equilibria equations (eqs 31−35) as in the theory for LbL deposition (with the obvious difference that all dependence of z is lost). Replacing all these expressions into the free energy functional, we obtain a simplified expression for the grand free energy density of the system equilibrium:

$$\frac{\beta\omega}{V} = -\beta p = -\sum_{\substack{i=A,B,s,H^+,\\ OH^-,Na^+,Cl^-}} \rho_i + N\rho_A f_{as}^A + \frac{1}{v_s}\ln(\rho_s v_s) + \frac{1}{2}\beta\epsilon g_{tot} N^2(\rho_A + \rho_B)^2 \quad (44)$$

where p is the thermodynamic pressure, and we used the fact that $\beta\omega = -\beta pV$ in the first equality. Using these expressions, we can now predict the phase diagram of the system.

2.5. Construction of the Binodal Phase Diagram. We calculate the binodal phase diagram of the system, in which the homogeneous phase is unstable if its decomposition into two phases leads to a decrease in the total free energy. In that condition, the chemical potentials of all species and the thermodynamic pressure in the two coexisting phases should be the same. There are additional constraints resulting from electroneutrality and the water self-dissociation equilibrium in both phases. In the Supporting Information, we discuss in detail the construction of the phase diagrams. The analysis is greatly simplified because in the experimental phase diagrams that we aim to describe, both PEs have the same chain length and concentration (this situation is in fact very common in experiments[10−12,23,60,61]). We also assume that the ion−polyion association constants for the Pol-A^-Na^+ and Pol-BH^+Cl^- are the same: ${}^AK_{as\text{-}ion} = {}^BK_{as\text{-}ion} = K_{as\text{-}ion}$. Finally, we analyze plots measured at neutral pH (pH = 7), where the concentrations of protons and hydroxyl ions are the same. All these considerations lead to very symmetric conditions, where the Donnan potential difference between the coexisting phases, $\Delta\phi = \phi^\alpha - \phi^\beta$, vanishes. This result (demonstrated in the Supporting Information) greatly simplifies the construction of the phase diagram. (Note that in the most general asymmetric case $\Delta\phi$ is nonzero, and thus it is an unknown variable.[45]) The construction of the phase diagram also benefits from if all ions and the solvent have the same molecular volume ($v_{Na^+} = v_{Cl^-} = v_s$), which is a very good approximation (see Figure S2).

2.6. Molecular Model. The input parameters for the MOLT include the solution properties (pH and salt concentration), the molecular properties of all species (i.e., the molecular model), and a set of randomly generated chain conformations. Note that we used exactly the same molecular model for both PE mixtures in solution and LbL films. The molecular volume of the solvent and all smalls ions (Na^+, Cl^-, H^+, and OH^-) was set to 0.03 nm^3. The molecular volume of the polymer segments, the association constants for the formation of ion−polyion (eqs 9 and 10) and polyion−polyion (eq 8) pairs, and the vdW interaction parameter ϵ were obtained from fitting the phase diagrams in solution (see discussion below). The acid−base constants for the acid and basic groups in the PEs were fixed to the typical values of carboxylates and amine groups in bulk solution, ${}^Ap K_a = 4.8$ and ${}^Bp K_a = 9.8$, respectively. Finally, the set of chain conformations need by the theory was randomly generated by using the rotational isomeric state model (RIS)[62] with a segment length of 0.35 nm.

3. RESULTS

3.1. Binodal Phase Diagrams of PE Mixtures in Solution. Figure 2 shows the predicted binodal diagram in the salt concentration vs total polymer concentration plane. The solid symbols show experimental results from Spruijt et al. for poly(acrylic acid)/poly(*N*,*N*-dimethylaminoethyl methacrylate) (PAA/PDMAEMA)[10] (Figure 2a) and Li et al. for poly(lysine)/poly(glutamic acid)[11] (Figure 2b). In both cases, each set of symbols corresponds to a different PE chain length. Our theoretical fittings are shown in solid lines. The fitting parameters in our theory are the equilibrium constants for the ion-pairing chemical reactions (K_{as} for polyion−polyion pairing and $K_{as\text{-}ion}$ for ion−polyion pairing), the molecular volume of the PE monomers (v_p), and the strength of the vdW interactions (ϵ). Note that while v_p was used as a fitting parameter, its value was constrained to lie in a reasonable range, 0.1−0.2 nm^3. In the fittings in Figure 2, we used v_p = 0.15 nm^3 for the monomers in PAA and PDMAEMA and v_p = 0.2 nm^3 for the (bulkier) glutamic acid and lysine monomers in poly(lysine) and poly(glutamic acid). Even with this constraint, there are different combinations of the four fitting parameters (K_{as}, $K_{as\text{-}ion}$, ϵ, and v_p) that can fit our results. Combinations with $\epsilon = 0$ (no vdW interactions, see Figure S3) failed later to successfully predict LbL growth, so we finally settle to values of ϵ in the range 0.5−1 k_BT/segment. Following these considerations, we obtained the values of all fitting parameters that are listed in the caption of Figure 2. The value of $K_{as\text{-}ion}$ (1.2 [M^{-1}]) is slightly larger than that previously obtained by MD simulations of 0.123 [M^{-1}] for carboxylate−Na^+ pairs.[63] However, it is important to mention that the values of K_{as} and $K_{as\text{-}ion}$ obtained from fitting experimental data with our theory may depend to some extent on the approximations used in its formulation; therefore, we recommend these constants to be used within the same theoretical framework (for example, in theory for LbL deposition discussed below or that in our previous work for mixed polycation/polyanion brushes[37]).

3.2. LbL Deposition. In the previous section, we demonstrated that our theory can correctly describe PE complexation in solution. We will now use the set of parameters obtained by fitting the experimental phase diagrams to model LbL deposition onto a surface. Hereafter, we use the set of parameters obtained from the data of Spruijt et al. (Figure 2a). The concentration of the PE being adsorbed is fixed to 0.02 M (in monomer units), a typical value used in

https://doi.org/10.1021/acs.macromol.2c00250
Macromolecules 2022, 55, 5263−5275

experiments.[17] Because the molecular theory uses explicit chain conformations, it is restricted to rather short chain lengths; thus, we used $N = 75$ for both PEs, which is in the lower range of those used for LbL self-assembly (∼100−10000 monomers/chain).

Figure 3a shows the volume fraction of the PE adsorbed in each LbL step as a function of the distance to the surface for

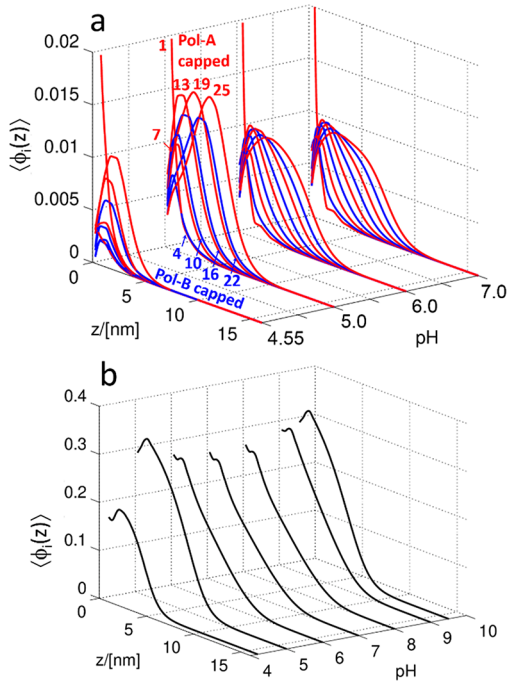

Figure 3. (a) Volume fractions of Pol-A (red lines) and Pol-B (blue lines) vs distance from the surface for LbL deposition at different deposition pHs. Each curve corresponds to a different layer. Only one in every three layers is shown (the number of layers is indicated next to each curve). (b) Total volume fraction of PEs (sum over all adsorbed layers) vs distance from the surface for LbL deposition at different deposition pHs for a 25-layer film. Calculation parameters: added salt concentration = 5 mM, chain length $N = 75$; $K_{as} = 3.55$ [M^{-1}]; $K_{as\text{-}ion} = 1.20$ [M^{-1}]; $\epsilon = 0.58\ k_BT$; $\nu_p = 0.15$ nm^3; $pK_a^A = 4.8$ and $pK_a^B = 9.8$.

LbL films deposited at different pHs and a constant concentration of added salt of 5 mM. The first important observation is that our theory, parametrized by using the phase behavior of PE mixtures in solution, can successfully predict LbL growth. While qualitatively correct, there are some quantitative differences between our predictions and experimental measurements. The volume fraction profiles in Figure 3a show a stronger interpenetration than that observed in experiments,[1] and the total PE volume fraction within the films (Figure 3b) is approximately half of that experimentally.[64] The short chains used in the calculations may contribute to these discrepancies, but we believe that interpenetration might be artificially enhanced in our model by the fact that we do not allow for PE reorganization after adsorption (i.e., PE layers are frozen in the rising step). Note that in experiments PE dangling chains in the topmost layer may collapse upon the addition of a subsequent layer of the oppositely charged polyion. This mechanism does not operate in our model, which thus may favor interpenetration.

3.3. Effect of pH on LbL Adsorption. Let us focus on the effect of the adsorption pH. Figure 3a only shows data for pH < 7 because the system is approximately symmetric around that pH. Figure 3 shows that the volume fractions of PE layers are largest at pH 5. This result is confirmed by Figure 4, which

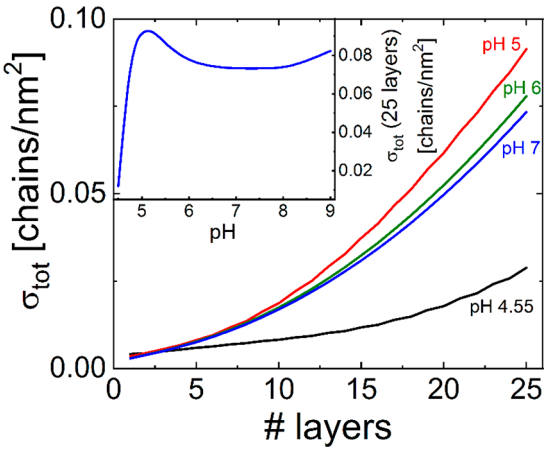

Figure 4. Total surface coverage of PE chains (σ_{tot}) as a function of the number of adsorbed layers for different adsorption pHs. Inset: σ_{tot} for 25 adsorbed layers vs pH. Same calculation conditions as in Figure 3.

shows that the total surface density of adsorbed chains as a function of the number of adsorbed layers. In fact, the inset of Figure 4 (which shows the total adsorbed surface density of PE chain vs pH for a 25-layer film) shows that total amount of adsorbed PE has two maxima: at pH ∼ 5 and 9. These maxima correspond to conditions where the polyacid and the polybase are partially charged, respectively. The presence of the two maxima was also observed in the classic work of Shiratori and Rubner, who studied the effect of pH on the film thickness of PAA/PAH films.[14] The effect of pH on film thickness observed in the experiment is more dramatic than that predicted in Figures 3 and 4. Reducing our chain length from $N = 75$ to $N = 20$ decreases in the magnitude of the predicted effect (see Figure S4), so we ascribe the quantitative difference between theory and experiment to the fact that we used shorter chains than the experimental ones. The effect of chain length is in line with the mechanism proposed for the effect of pH on film thickness.[14] At pH ∼ 7, both PEs are fully charged, so they adopt rodlike conformations in solution that lay flat on the surface and lead to thin films. At pH 5 and 9, one of the PEs is partially charged, so it adopts a coiled conformation that gives rise to thick films. However, because N is small in our case, the sizes of coiled and uncoiled chains do not strongly differ, which explains the difference in the magnitude of the effect of pH between theory and experiment.

The results in Figures 3 and 4 show that at low pH (pH ∼ 4.5), where the polyacid is mainly protonated, the total amount of adsorbed PE starts to decline. In this case, there is a competition between the acid−base reaction (protonation of the polyacid) and the ion-pairing association. In other words, protonated acid groups, which form at low pH, are not available to form ion pairs with the positive groups of the polybase. This mechanism is supported by the data in Figure S5, which shows that at pH < 5 the fraction of associated monomers (for both polyion−polyion and polyion−ion pairs) decreases because of the increase of the fraction of protonated (uncharged) acid groups.

https://doi.org/10.1021/acs.macromol.2c00250
Macromolecules 2022, 55, 5263−5275

3.4. Charge Reversal during LbL Deposition. Figure 5 shows the electrostatic potential profile for different pH

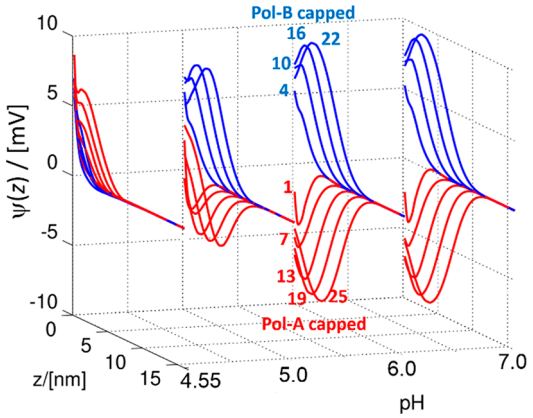

Figure 5. Electrostatic potential profiles predicted during the adsorption of Pol-A (red lines) and Pol-B (blue lines) at different deposition pHs and number of adsorbed layers. Only one in every three layers is shown (the number of layers is indicated next to each curve). Same calculation conditions as in Figure 3.

conditions and number of adsorbed layers. At pH = 7, there is an evident alternation between positive and negative potentials for Pol-B and Pol-A capped films, respectively, a phenomena commonly known as charge reversal.[2] The maxima (for Pol-B capped multilayers) and minima (for Pol-A capped films) of the electrostatic potential profiles shift to larger z as the number of layers increase. This result agrees with the accepted description of the structure of LbL films in which the interior of the film is electrically neutral, and the excess charge is mainly located at the film/solution interface.[2]

As the deposition pH decreases, Figure 5 shows that the magnitude of the minimum of the electrostatic potential for Pol-A-capped films starts to decrease. For pH = 4.5, the electrostatic potential is positive for both Pol-A and Pol-B capped multilayers; however, Figures 3 and 4 show that film growth still occurs at this pH (although at a slower rate than for pH 5). This result indicates that full charge reversal is not required for multilayer growth. Notably, there exists experimental studies where charge reversal is not observed.[65−68] For example, Richter et al.[65] studied the streaming potential during the deposition of poly(L-lysine)/poly(L-glutamic acid) LbL films. For neutral pH (7.4), the surface potential oscillated between negative and positive values; however, for pH = 4.4, the potential was always positive, and for basic pH (10.4) the potential was always negative. These experimental observations indicate that charge reversal in not requisite for successful LbL growth and agree remarkably well with the predictions of our theory for pH 4.55.

LbL deposition in the absence of charge reversal can be explained in terms of the chemical equilibria considered by our theory. At pH 4.55, the adsorption of Pol-A on top of a Pol-B-capped film does not invert the surface charge because Pol-A is strong protonated (uncharged) at that pH. However, in the next adsorption step, Pol-B can still adsorb on the Pol-A-capped multilayer because the formation of polyion−polyion ion pairs can displace the acid−base equilibria of the acid groups, i.e.

$$\text{Pol-AH}_{(\text{sol})} + \text{Pol-BH}^{+}_{(\text{film})} \rightleftarrows [\text{Pol-A}^{-}\text{Pol-BH}^{+}]_{(\text{film})} + \text{H}^{+}_{(\text{sol})} \quad (45)$$

This charge-regulation mechanism is apparent in Figure S5, which shows that the average fraction of charged A^- groups in Pol-A at pH = ${}^{A}pK_a$ = 4.8 is ∼0.37 instead of the value of 0.5 expected for free A^-/HA species in solution. It also qualitatively agrees with experimental measurements that have shown that the pK_a of PAA within LbL films is smaller than that of PAA free in solution.[69] This result also reinforces our claim that long-range electrostatics is not enough to describe LbL growth, but rather the formation of ion pairs and the entropic contribution of counterion release are needed. Nonetheless, the adsorption of Pol-B onto a positively charged multilayer is still electrostatically penalized, which explains why the amount of adsorbed chains rapidly declines when lowering the pH below 5 (see Figure 4).

3.5. Effect of Salt Concentration. In addition to the solution pH, the other variable that exerts a strong influence over the LbL adsorption process is the ionic strength of the solution. Figure 6a shows volume-fraction profiles for different number of adsorbed layers and different ionic strengths and fixed pH = 7. Figure 6b shows a summary of these results in the form of plots of the total number of adsorbed chains vs adsorption step, and the inset of the figure shows how this parameter changes with the salt concentration for a fixed

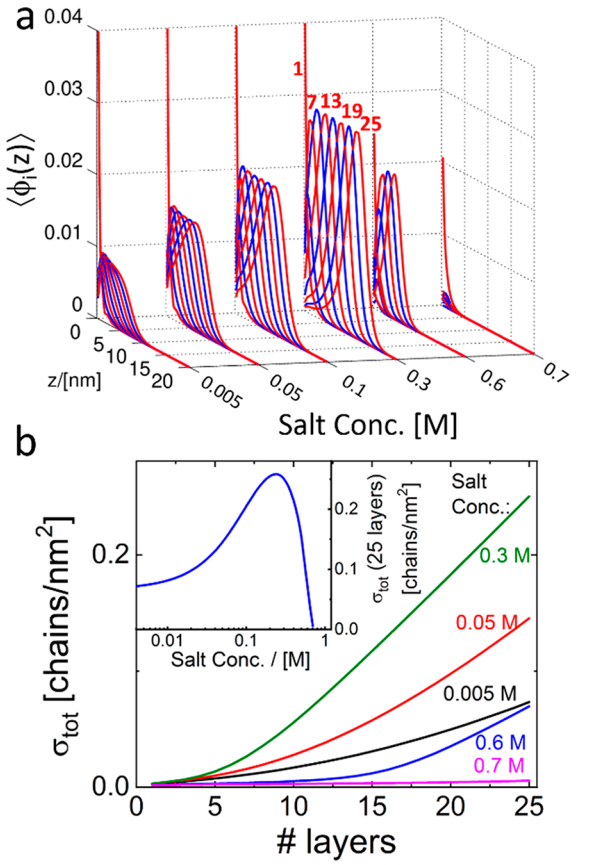

Figure 6. (a) Volume fractions of Pol-A (red lines) and Pol-B (blue lines) vs distance from the surface for LbL deposition at different salt concentrations. Each curve corresponds to a different layer. Only one in every three layers is shown (the number of layers is indicated next to each curve). Figure S7 shows a 2D plot of the data for C_{salt} = 0.3 M. (b) Total surface coverage of PE chains (σ_{tot}) as a function of the number of adsorbed layers for different concentrations of added salt. Inset: σ_{tot} for 25 adsorbed layers vs concentration of added salt. Same calculation conditions as in Figure 3 and pH = 7.

https://doi.org/10.1021/acs.macromol.2c00250
Macromolecules 2022, 55, 5263−5275

number of adsorbed layers. The most salient feature of these calculations is that the amount of adsorbed PEs experiences a maximum around c_{salt} = 0.25 M (see the inset in Figure 6b). Similar maxima in film thickness vs salt concentration (in the range of c_{salt} = 0.1−0.3 M) were observed for many LbL films containing the same polyanion used to parametrize our model, PAA.[16,22]

The initial increase in the amount of deposited PE with salt concentration shown in Figure 6 may seem puzzling because of the role of salt in the dissociation of polyion−polyion bonds. It has been argued[19] that large salt concentration favors coiled conformations in solution, which in turn produces thick films. As discussed above, this mechanism is not likely to be dominant in our calculations because our PE chains are short. In our case, the origin of the maximum can be traced back to the competition between long-range electrostatics and ion pairing. At low salt concentration and pH = 7, the charge of a PE can only be compensated via the formation of complexes with the oppositely charged polyion. In addition, the screening of PE charges by salt is very inefficient at low ionic strength. In these conditions, a small overcompensation of the film charge results in large and sudden reversal of the electrostatic potential. Note the electrostatic potentials of films deposited at c_{salt} = 5 mM display the strongest oscillations with the number of layers in Figure 7, even though the PE mass

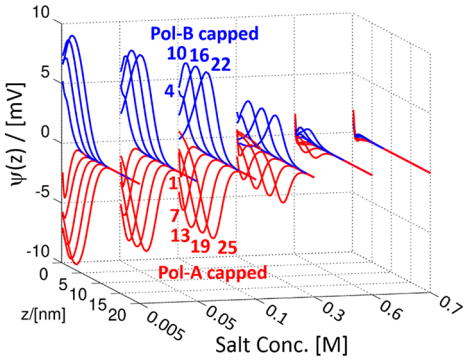

Figure 7. Electrostatic potential profiles for the adsorption of Pol-A (red lines) and Pol-B (blue lines) at different salt concentrations and number of adsorbed layers. Only one in every three layers is shown (the number of layers is indicated next to each curve). Same calculation conditions as in Figure 3 and pH = 7.

deposited in adsorption each step in for c_{salt} = 5 mM is the smallest in Figure 6. The strong and sudden reversal of the electrostatic potential hinders further PE adsorption, and thus, LbL growth is inefficient at low ionic strength. We stress that the success of our theory to capture the initial increase of the deposited mass with salt concentration results from the competition of short-range electrostatic attractions (modeled as ion-association equilibria) and long-range electrostatic repulsions (given by the generalized Poisson equation, eq 19). Thus, both contributions are necessary to correctly describe LbL deposition.

As the ionic strength approaches its optimal value (∼0.25 M, see Figure 6b), salt screens the charge of the PEs and further reduces it via the formation of polyion−ion pairs. When the ionic strength is increased beyond 0.25 M, the formation of polyion−polyion pairs becomes inhibited by the presence of polyion−ion pairs, PE chains become weakly absorbed and can be removed during the rising step, and therefore the mass of PE adsorbed in each LbL step rapidly decrease with increasing salt concentration.

The salt concentration is very important in determining the growing mechanism of the film.[16] The thickness of layer-by-layer films can growth either linearly or exponentially with the number of adsorption steps. Exponential growth has been explained by considering that PE chains diffuse into the film. During the adsorption of the following layer, these PE chains diffuse out of the film and form a complex with the oppositely charged polyion at the solution/film interface.[70−72] Salehi et al. observed that the growing mechanism changes from linear to exponential and then back to linear with increasing salt concentration.[16] In our case, we observe a transition from linear to faster-than-linear growth at ∼0.4 M (see Figure S6). This transition occurs at a higher salt concentration than that reported by Salehi et al. (see discussion in the Supporting Information), and our theory fails to predict the second linear regime. These discrepancies are probably originated in the approximation used in our model of freezing the density profiles of previously adsorbed layers. In other words, our model allows the diffusion of PE chains into the film (i.e., we do not impose a hard wall like some previous models[49,50]), and therefore it can predict nonlinear growth to some extent. However, freezing the density profiles after each adsorption step prevents polyelectrolyte chains adsorbed in one step to diffuse out in the following one, and therefore our model does not quantitatively capture the effect of salt concentration on the exponential growth mechanism discussed above.

3.6. Revisiting the Universal Curve for the Effect of Salt Concentration on LbL Adsorption. The main advantage of having a unified theory for PE coacervation in solution and LbL multilayer films resides in exploring the connections between these two phenomena. As an example, in this section we revisit the universal curve for the effect of salt concentration on LbL growth, previously suggested by Salehi et al.[16] These authors measured, for three different PE pairs, both the critical salt concentration from phase diagrams in solution (c_{salt}^{crit}, i.e., the maximum salt concentration of the binodal curve, above which PE coacervates cannot exist; see Figure 2) and the mass of PEs deposited in LbL films as a function of salt concentration. They noted that the salt concentration exhibiting the fastest LbL growth increased with increasing c_{salt}^{crit}. Even more interestingly, by normalizing the PE mass deposited in LbL films and dividing the salt concentration by c_{salt}^{crit}, Salehi et al. were able to overlay their three experimental data sets, collapsing their data into a single universal curve.

To theoretically validate the concept of the universal curve, we performed MOLT calculations for phase diagrams in solution and LbL deposition using different combinations of K_{as}, $K_{as\text{-}ion}$, and N (see Figure 8a). We then performed the normalization proposed by Salehi et al., which collapsed all our data sets into a single curve (see Figure 8b). Moreover, the previous experimental points of Salehi et al. lay on the same curve. These results strongly support the idea that this curve is universal and independent of specific choice of the PE pair.

4. CONCLUSIONS

This work introduced a molecular theory to describe both the phase diagrams of PE mixtures in solution and their LbL deposition. The theory describes the formation of ion pairs responsible for PE complexation by using chemical equilibria reactions. This concept was already exploited in the

https://doi.org/10.1021/acs.macromol.2c00250
Macromolecules 2022, 55, 5263−5275

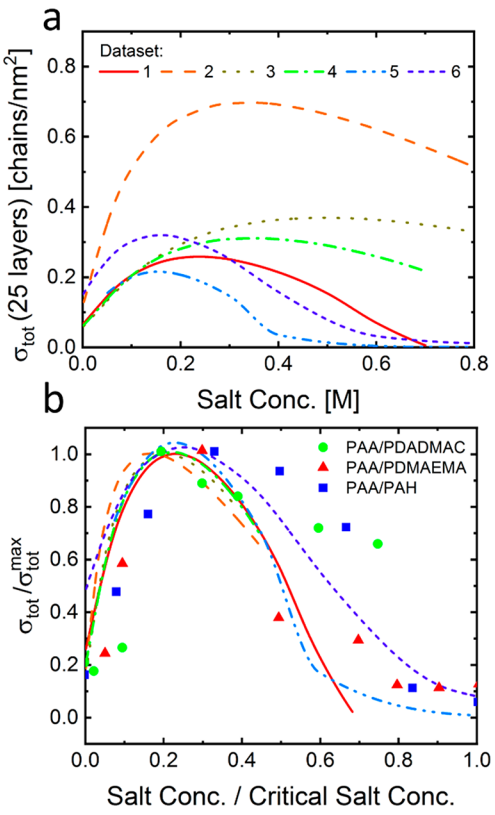

Figure 8. (a) Total surface coverage of PE chains for a 25-layer film vs concentration of added salt (same plot as in the inset of Figure 6b) for data sets by using different calculation parameters. K_{as} = 3.55 [M^{-1}] (sets 1, 3–6) or 8.91 [M^{-1}] (set 2); $K_{as\text{-}ion}$ = 1.20 [M^{-1}] (sets 1, 2, 6), 0.48 [M^{-1}] (set 3), 0.76 [M^{-1}] (set 4) or 1.91 [M^{-1}] (set 5), N = 75 (sets 1–5) or 20 (set 6). Other calculation parameters were as in Figure 3 and pH = 7. (b) Universal curve obtained by normalizing the amount of deposited PE of each curve in panel a by its maximum and dividing the concentration of added salt by the critical concentration obtained from predicted phase diagrams for each set of parameters. Symbols show the experimental data of Salehi et al.,[16] and lines show the predictions of our theory for the same data sets shown in (a).

literature,[28−30,37,46] but in this work, we used it for the first time to model LbL adsorption. The equilibrium formalism is very intuitive and conceptually simple, although it requires to parametrize the values of the equilibrium constants. We obtained the equilibrium constants for polyion−polyion and ion−polyion association by fitting experimental phase diagrams for PE mixtures in solution and then used them to model the deposition of multilayer films. While the chemical equilibrium formalism was used in previous works to fit the phase diagram of coacervates in solution,[12,46] this is the first time that the as-obtained binding constants are used to model a different (albeit related) phenomena: LbL deposition. Describing both PE coacervation and LbL deposition within the same theoretical framework is important to establish links between both phenomena. We showed that the predictions of our theory follow accurately the universal curve previously proposed by Salehi, Larson, and co-workers for the effect of salt on LbL deposition, thus confirming its validity. This universal curve is useful because it allows to estimate the optimal salt concentration for LbL assembly from the behavior of a PE mixture in solution.

Our predictions for LbL assembly simultaneously captured many interesting trends previously observed in experiments. For example, our model correctly predicted the effects of salt concentration and solution pH on LbL deposition, while previous theoretical work in the field addressed either one or the other.[41,48−50] A more intriguing prediction is the possibility of multilayer growth without full charge reversal, which was experimentally observed[65−68] but not predicted theoretically before this work. Despite the success of our theory to qualitatively capture LbL growth and some experimental trends, some of our predictions still differ quantitatively with experiments, so there is ample room for improvement. For example, the predicted PE volume fraction in the film (∼0.2−0.25; see Figure 3b) is smaller than that measured in experiments,[64] and our density profiles suggest a much stronger interpenetration than that experimentally observed.[1] Among the potential causes for these discrepancies, we can mention the short chain lengths used in our theory and the lack of relaxation of previously deposited layers. We seek to improve some of these issues in the further developments of the theory. We are also interested in applying our theory to other closely related problems, such as asymmetric PE coacervates and salt−polyamine complexes,[73,74] where the two species forming the aggregates have markedly different molecular weights, concentrations, and/or charge fractions.

■ ASSOCIATED CONTENT

Supporting Information

The Supporting Information is available free of charge at https://pubs.acs.org/doi/10.1021/acs.macromol.2c00250.

Effect of N_b^{max} on PE volume fraction profiles, detailed description of the construction of the binodal phase diagrams, effect of the molecular volume of salt ions on the binodal phase diagrams, fitting of the binodal phase diagrams without vdW attractions, effect of chain length on pH-dependent LbL adsorption and fraction of PE monomers in the different chemical states within LbL films, discussion of the growing mechanism (PDF)

■ AUTHOR INFORMATION

Corresponding Author

Mario Tagliazucchi − *Facultad de Ciencias Exactas y Naturales, Departamento de Química Inorgánica Analítica y Química Física, Universidad de Buenos Aires, C1053ABH Buenos Aires, Argentina; Facultad de Ciencias Exactas y Naturales, CONICET- Universidad de Buenos Aires, C1053ABH Buenos Aires, Argentina;* orcid.org/0000-0003-4755-955X; Email: mario@qi.fcen.uba.ar

Author

Gabriel Debais − *Facultad de Ciencias Exactas y Naturales, Departamento de Química Inorgánica Analítica y Química Física, Universidad de Buenos Aires, C1053ABH Buenos Aires, Argentina; Facultad de Ciencias Exactas y Naturales, CONICET- Universidad de Buenos Aires, C1053ABH Buenos Aires, Argentina*

Complete contact information is available at: https://pubs.acs.org/10.1021/acs.macromol.2c00250

Notes

The authors declare no competing financial interest.

https://doi.org/10.1021/acs.macromol.2c00250
Macromolecules 2022, 55, 5263−5275

■ ACKNOWLEDGMENTS

M.T. is a fellow of CONICET. M.T. acknowledges financial support from Agencia Nacional de Promoción Científica y Tecnológica (ANPCyT) PICT 4649-2018 and PICT 1520-2019 and CONICET PIP 11220200102008CO.

■ ABBREVIATIONS

PE, polyelectrolyte; LbL, layer-by-layer; MOLT, molecular theory.

■ REFERENCES

(1) Decher, G. Fuzzy Nanoassemblies: Toward Layered Polymeric Multicomposites. *Science* **1997**, *277* (5330), 1232−1237.
(2) Decher, G.; Schlenoff, J. B. *Multilayer Thin Films: Sequential Assembly of Nanocomposite Materials*; John Wiley & Sons: 2006.
(3) Hammond, P. T. Form and Function in Multilayer Assembly: New Applications at the Nanoscale. *Adv. Mater.* **2004**, *16* (15), 1271−1293.
(4) Schönhoff, M. Self-Assembled Polyelectrolyte Multilayers. *Curr. Opin. Colloid Interface Sci.* **2003**, *8* (1), 86−95.
(5) Sing, C. E.; Perry, S. L. Recent Progress in the Science of Complex Coacervation. *Soft Matter* **2020**, *16* (12), 2885−2914.
(6) Srivastava, S.; Tirrell, M. V. Polyelectrolyte Complexation. *Adv. Chem. Phys.* **2016**, *161*, 499−544.
(7) Van der Gucht, J.; Spruijt, E.; Lemmers, M.; Stuart, M. A. C. Polyelectrolyte Complexes: Bulk Phases and Colloidal Systems. *J. Colloid Interface Sci.* **2011**, *361* (2), 407−422.
(8) Rumyantsev, A. M.; Jackson, N. E.; De Pablo, J. J. Polyelectrolyte Complex Coacervates: Recent Developments and New Frontiers. *Annu. Rev. Condens. Matter Phys.* **2021**, *12*, 155−176.
(9) Spruijt, E.; Cohen Stuart, M. A.; van der Gucht, J. Dynamic Force Spectroscopy of Oppositely Charged Polyelectrolyte Brushes. *Macromolecules* **2010**, *43* (3), 1543−1550.
(10) Spruijt, E.; Westphal, A. H.; Borst, J. W.; Cohen Stuart, M. A.; van der Gucht, J. Binodal Compositions of Polyelectrolyte Complexes. *Macromolecules* **2010**, *43* (15), 6476−6484.
(11) Li, L.; Srivastava, S.; Andreev, M.; Marciel, A. B.; de Pablo, J. J.; Tirrell, M. V. Phase Behavior and Salt Partitioning in Polyelectrolyte Complex Coacervates. *Macromolecules* **2018**, *51* (8), 2988−2995.
(12) Lou, J.; Friedowitz, S.; Qin, J.; Xia, Y. Tunable Coacervation of Well-Defined Homologous Polyanions and Polycations by Local Polarity. *ACS Cent. Sci.* **2019**, *5* (3), 549−557.
(13) Perry, S. L.; Li, Y.; Priftis, D.; Leon, L.; Tirrell, M. The Effect of Salt on the Complex Coacervation of Vinyl Polyelectrolytes. *Polymers* **2014**, *6* (6), 1756−1772.
(14) Shiratori, S. S.; Rubner, M. F. PH-Dependent Thickness Behavior of Sequentially Adsorbed Layers of Weak Polyelectrolytes. *Macromolecules* **2000**, *33* (11), 4213−4219.
(15) Tagliazucchi, M.; Williams, F. J.; Calvo, E. J. Effect of Acid-Base Equilibria on the Donnan Potential of Layer-by-Layer Redox Polyelectrolyte Multilayers. *J. Phys. Chem. B* **2007**, *111* (28), 8105−8113.
(16) Salehi, A.; Desai, P. S.; Li, J.; Steele, C. A.; Larson, R. G. Relationship between Polyelectrolyte Bulk Complexation and Kinetics of Their Layer-by-Layer Assembly. *Macromolecules* **2015**, *48* (2), 400−409.
(17) Dubas, S. T.; Schlenoff, J. B. Factors Controlling the Growth of Polyelectrolyte Multilayers. *Macromolecules* **1999**, *32* (24), 8153−8160.
(18) Guzmán, E.; Ritacco, H.; Rubio, J. E. F.; Rubio, R. G.; Ortega, F. Salt-Induced Changes in the Growth of Polyelectrolyte Layers of Poly(Diallyl-Dimethylammonium Chloride) and Poly(4-Styrene Sulfonate of Sodium). *Soft Matter* **2009**, *5* (10), 2130−2142.
(19) Liu, G.; Zou, S.; Fu, L.; Zhang, G. Roles of Chain Conformation and Interpenetration in the Growth of a Polyelectrolyte Multilayer. *J. Phys. Chem. B* **2008**, *112* (14), 4167−4171.
(20) Reurink, D. M.; Willott, J. D.; Roesink, H. D. W.; de Vos, W. M. Role of Polycation and Cross-Linking in Polyelectrolyte Multilayer Membranes. *ACS Appl. Polym. Mater.* **2020**, *2* (11), 5278−5289.
(21) Sui, Z.; Salloum, D.; Schlenoff, J. B. Effect of Molecular Weight on the Construction of Polyelectrolyte Multilayers: Stripping versus Sticking. *Langmuir* **2003**, *19* (6), 2491−2495.
(22) Dubas, S. T.; Schlenoff, J. B. Polyelectrolyte Multilayers Containing a Weak Polyacid: Construction and Deconstruction. *Macromolecules* **2001**, *34* (11), 3736−3740.
(23) Wang, Q.; Schlenoff, J. B. The Polyelectrolyte Complex/Coacervate Continuum. *Macromolecules* **2014**, *47* (9), 3108−3116.
(24) Ou, Z.; Muthukumar, M. Entropy and Enthalpy of Polyelectrolyte Complexation: Langevin Dynamics Simulations. *J. Chem. Phys.* **2006**, *124* (15), 154902.
(25) Cerda, J. J.; Qiao, B.; Holm, C. Understanding Polyelectrolyte Multilayers: An Open Challenge for Simulations. *Soft Matter* **2009**, *5* (22), 4412−4425.
(26) Fu, J.; Schlenoff, J. B. Driving Forces for Oppositely Charged Polyion Association in Aqueous Solutions: Enthalpic, Entropic, but Not Electrostatic. *J. Am. Chem. Soc.* **2016**, *138* (3), 980−990.
(27) Narambuena, C. F.; Beltramo, D. M.; Leiva, E. P. M. Polyelectrolyte Adsorption on a Charged Surface. Free Energy Calculation from Monte Carlo Simulations Using Jarzynski Equality. *Macromolecules* **2008**, *41* (21), 8267−8274.
(28) Schlenoff, J. B.; Ly, H.; Li, M. Charge and Mass Balance in Polyelectrolyte Multilayers. *J. Am. Chem. Soc.* **1998**, *120* (30), 7626−7634.
(29) Farhat, T. R.; Schlenoff, J. B. Doping-Controlled Ion Diffusion in Polyelectrolyte Multilayers: Mass Transport in Reluctant Exchangers. *J. Am. Chem. Soc.* **2003**, *125* (15), 4627−4636.
(30) Jaber, J. A.; Schlenoff, J. B. Mechanical Properties of Reversibly Cross-Linked Ultrathin Polyelectrolyte Complexes. *J. Am. Chem. Soc.* **2006**, *128* (9), 2940−2947.
(31) Solis, F. J.; de la Cruz, M. O. Surface-Induced Layer Formation in Polyelectrolytes. *J. Chem. Phys.* **1999**, *110* (23), 11517−11522.
(32) Messina, R. Polyelectrolyte Multilayering on a Charged Planar Surface. *Macromolecules* **2004**, *37* (2), 621−629.
(33) Patel, P. A.; Jeon, J.; Mather, P. T.; Dobrynin, A. V. Molecular Dynamics Simulations of Multilayer Polyelectrolyte Films: Effect of Electrostatic and Short-Range Interactions. *Langmuir* **2006**, *22* (24), 9994−10002.
(34) Radhakrishna, M.; Basu, K.; Liu, Y.; Shamsi, R.; Perry, S. L.; Sing, C. E. Molecular Connectivity and Correlation Effects on Polymer Coacervation. *Macromolecules* **2017**, *50* (7), 3030−3037.
(35) Overbeek, J. T. G.; Voorn, M. Phase Separation in Polyelectrolyte Solutions. Theory of Complex Coacervation. *J. Cell. Comp. Physiol.* **1957**, *49* (S1), 7−26.
(36) Sing, C. E. Development of the Modern Theory of Polymeric Complex Coacervation. *Adv. Colloid Interface Sci.* **2017**, *239*, 2−16.
(37) Debais, G.; Tagliazucchi, M. Microphase Separation and Aggregate Self-Assembly in Brushes of Oppositely Charged Polyelectrolytes Triggered by Ion Pairing. *J. Chem. Phys.* **2020**, *153* (14), 144903.
(38) Castelnovo, M.; Joanny, J.-F. Complexation between Oppositely Charged Polyelectrolytes: Beyond the Random Phase Approximation. *Eur. Phys. J. E* **2001**, *6* (1), 377−386.
(39) Kudlay, A.; Ermoshkin, A. V.; Olvera de La Cruz, M. Complexation of Oppositely Charged Polyelectrolytes: Effect of Ion Pair Formation. *Macromolecules* **2004**, *37* (24), 9231−9241.
(40) Ermoshkin, A.; Olvera de La Cruz, M. A Modified Random Phase Approximation of Polyelectrolyte Solutions. *Macromolecules* **2003**, *36* (20), 7824−7832.
(41) Castelnovo, M.; Joanny, J. F. Formation of Polyelectrolyte Multilayers. *Langmuir* **2000**, *16* (19), 7524−7532.
(42) Delaney, K. T.; Fredrickson, G. H. Theory of Polyelectrolyte Complexation—Complex Coacervates Are Self-Coacervates. *J. Chem. Phys.* **2017**, *146* (22), 224902.

https://doi.org/10.1021/acs.macromol.2c00250
Macromolecules 2022, 55, 5263−5275

(43) Lee, J.; Popov, Y. O.; Fredrickson, G. H. Complex Coacervation: A Field Theoretic Simulation Study of Polyelectrolyte Complexation. *J. Chem. Phys.* **2008**, *128* (22), 224908.
(44) Perry, S. L.; Sing, C. E. PRISM-Based Theory of Complex Coacervation: Excluded Volume versus Chain Correlation. *Macromolecules* **2015**, *48* (14), 5040−5053.
(45) Zhang, P.; Alsaifi, N. M.; Wu, J.; Wang, Z.-G. Polyelectrolyte Complex Coacervation: Effects of Concentration Asymmetry. *J. Chem. Phys.* **2018**, *149* (16), 163303.
(46) Salehi, A.; Larson, R. G. A Molecular Thermodynamic Model of Complexation in Mixtures of Oppositely Charged Polyelectrolytes with Explicit Account of Charge Association/Dissociation. *Macromolecules* **2016**, *49* (24), 9706−9719.
(47) Friedowitz, S.; Salehi, A.; Larson, R. G.; Qin, J. Role of Electrostatic Correlations in Polyelectrolyte Charge Association. *J. Chem. Phys.* **2018**, *149* (16), 163335.
(48) Wang, Q. Internal Structure and Charge Compensation of Polyelectrolyte Multilayers: A Numerical Study. *Soft Matter* **2009**, *5* (2), 413−424.
(49) Shafir, A.; Andelman, D. Polyelectrolyte Multilayer Formation: Electrostatics and Short-Range Interactions. *Eur. Phys. J. E* **2006**, *19* (2), 155−162.
(50) Park, S. Y.; Rubner, M. F.; Mayes, A. M. Free Energy Model for Layer-by-Layer Processing of Polyelectrolyte Multilayer Films. *Langmuir* **2002**, *18* (24), 9600−9604.
(51) Subbotin, A. V.; Semenov, A. N. The Structure of Polyelectrolyte Complex Coacervates and Multilayers. *Macromolecules* **2021**, *54* (3), 1314−1328.
(52) Nap, R. J.; Tagliazucchi, M.; Szleifer, I. Born Energy, Acid-Base Equilibrium, Structure and Interactions of End-Grafted Weak Polyelectrolyte Layers. *J. Chem. Phys.* **2014**, *140* (2), 024910.
(53) Carignano, M. A.; Szleifer, I. Structure and Thermodynamics of Grafted Three-Arm Branched Polymer Layers. *Macromolecules* **1994**, *27* (3), 702−710.
(54) Zaldivar, G.; Tagliazucchi, M. Layer-by-Layer Self-Assembly of Polymers with Pairing Interactions. *ACS Macro Lett.* **2016**, *5*, 862−866.
(55) Tagliazucchi, M.; de la Cruz, M. O.; Szleifer, I. Self-Organization of Grafted Polyelectrolyte Layers via the Coupling of Chemical Equilibrium and Physical Interactions. *Proc. Natl. Acad. Sci. U. S. A.* **2010**, *107*, 5300−5305.
(56) Zaldivar, G.; Vemulapalli, S.; Udumula, V.; Conda-Sheridan, M.; Tagliazucchi, M. Self-Assembled Nanostructures of Peptide Amphiphiles: Charge Regulation by Size Regulation. *J. Phys. Chem. C* **2019**, *123* (28), 17606−17615.
(57) Nap, R.; Gong, P.; Szleifer, I. Weak Polyelectrolytes Tethered to Surfaces: Effect of Geometry, Acid-Base Equilibrium and Electrical Permittivity. *J. Polym. Sci., Part B: Polym. Phys.* **2006**, *44*, 2638−2662.
(58) Danielsen, S. P. O.; Panyukov, S.; Rubinstein, M. Ion Pairing and the Structure of Gel Coacervates. *Macromolecules* **2020**, *53* (21), 9420−9442.
(59) Rubinstein, M.; Liao, Q.; Panyukov, S. Structure of Liquid Coacervates Formed by Oppositely Charged Polyelectrolytes. *Macromolecules* **2018**, *51* (23), 9572−9588.
(60) Kim, S.; Lee, M.; Lee, W. B.; Choi, S.-H. Ionic-Group Dependence of Polyelectrolyte Coacervate Phase Behavior. *Macromolecules* **2021**, *54*, 7572.
(61) Li, L.; Srivastava, S.; Meng, S.; Ting, J. M.; Tirrell, M. V. Effects of Non-Electrostatic Intermolecular Interactions on the Phase Behavior of PH-Sensitive Polyelectrolyte Complexes. *Macromolecules* **2020**, *53* (18), 7835−7844.
(62) Rubinstein, M.; Colby, R. H. *Polymer Physics*; Oxford University Press.
(63) Nap, R. J.; Park, S. H.; Szleifer, I. On the Stability of Nanoparticles Coated with Polyelectrolytes in High Salinity Solutions. *J. Polym. Sci., Part B: Polym. Phys.* **2014**, *52* (24), 1689−1699.
(64) Carriere, D.; Krastev, R.; Schönhoff, M. Oscillations in Solvent Fraction of Polyelectrolyte Multilayers Driven by the Charge of the Terminating Layer. *Langmuir* **2004**, *20* (26), 11465−11472.
(65) Richert, L.; Arntz, Y.; Schaaf, P.; Voegel, J.-C.; Picart, C. PH Dependent Growth of Poly (L-Lysine)/Poly (L-Glutamic) Acid Multilayer Films and Their Cell Adhesion Properties. *Surf. Sci.* **2004**, *570* (1−2), 13−29.
(66) Adusumilli, M.; Bruening, M. L. Variation of Ion-Exchange Capacity, ζ Potential, and Ion-Transport Selectivities with the Number of Layers in a Multilayer Polyelectrolyte Film. *Langmuir* **2009**, *25* (13), 7478−7485.
(67) Reurink, D. M.; Haven, J. P.; Achterhuis, I.; Lindhoud, S.; Roesink, H.; de Vos, W. M. Annealing of Polyelectrolyte Multilayers for Control over Ion Permeation. *Adv. Mater. Interfaces* **2018**, *5* (20), 1800651.
(68) Riegler, H.; Essler, F. Polyelectrolytes. 2. Intrinsic or Extrinsic Charge Compensation? Quantitative Charge Analysis of PAH/PSS Multilayers. *Langmuir* **2002**, *18* (17), 6694−6698.
(69) Choi, J.; Rubner, M. F. Influence of the Degree of Ionization on Weak Polyelectrolyte Multilayer Assembly. *Macromolecules* **2005**, *38* (1), 116−124.
(70) Lavalle, P.; Picart, C.; Mutterer, J.; Gergely, C.; Reiss, H.; Voegel, J.-C.; Senger, B.; Schaaf, P. Modeling the Buildup of Polyelectrolyte Multilayer Films Having Exponential Growth. *J. Phys. Chem. B* **2004**, *108* (2), 635−648.
(71) Hoda, N.; Larson, R. G. Modeling the Buildup of Exponentially Growing Polyelectrolyte Multilayer Films. *J. Phys. Chem. B* **2009**, *113* (13), 4232−4241.
(72) Picart, C.; Mutterer, J.; Richert, L.; Luo, Y.; Prestwich, G. D.; Schaaf, P.; Voegel, J.-C.; Lavalle, P. Molecular Basis for the Explanation of the Exponential Growth of Polyelectrolyte Multilayers. *Proc. Natl. Acad. Sci. U. S. A.* **2002**, *99* (20), 12531−12535.
(73) Herrera, S. E.; Agazzi, M. L.; Cortez, M. L.; Marmisollé, W. A.; Tagliazucchi, M.; Azzaroni, O. Multitasking Polyamine/Ferrioxalate Nano-Sized Assemblies: Thermo-, Photo-, and Redox-Responsive Soft Materials Made Easy. *Chem. Commun.* **2019**, *55* (97), 14653−14656.
(74) Herrera, S. E.; Agazzi, M. L.; Cortez, M. L.; Marmisollé, W. A.; Tagliazucchi, M.; Azzaroni, O. Redox-Active Polyamine-Salt Aggregates as Multistimuli-Responsive Soft Nanoparticles. *Phys. Chem. Chem. Phys.* **2020**, *22* (14), 7440−7450.

https://doi.org/10.1021/acs.macromol.2c00250
Macromolecules 2022, 55, 5263−5275